Optimized extraction, quantification and characterization of seven environmentally relevant metallic nanoparticles in sewage sludge: Occurrence, composition and environmental risk assessment

Mavro Lučić[1,3]*, Radmila Milačič Ščančar[1,2], Janez Ščančar[1,2], Željka Fiket[3], Bor Arah[4], Janja Vidmar[1,2]*

[1]Department of Environmental Sciences, Jožef Stefan Institute, Jamova 39, Ljubljana, Slovenia

[2]Jožef Stefan International Postgraduate School, Jamova 39, 1000 Ljubljana, Slovenia

[3]Division for Marine and Environmental Research, Ruder Bošković Institute, Bijenička cesta 54, Zagreb, Croatia

[4]Center for Electron Microscopy and Microanalysis, Jožef Stefan Institute, Jamova 39, Ljubljana, Slovenia

*Corresponding authors:

mlucic@irb.hr

janja.vidmar@ijs.si

Abstract

The quantitative analysis of metallic nanoparticles (MNPs) in environmental matrices is crucial for understanding their occurrence, fate, and ecological risks. This study presents an optimized protocol for extracting and quantifying seven of the most commonly used MNPs (Ag, Au, CeO_2, CuO, PbO, TiO_2 and ZnO) from sewage sludge using single-particle inductively coupled plasma mass

spectrometry (sp-ICP-MS). Several extraction parameters and solutions, including milli-Q water, tetrasodium pyrophosphate (TSPP), and tetramethylammonium hydroxide (TMAH), were systematically evaluated. TSPP at 2.5 mM in a 1:100 sludge-to-reagent ratio was identified as the optimal extraction solution, providing high particle number recovery (>75%) and mass recovery (>84.5%) while minimizing particle transformation. Application to sludge samples from wastewater treatment plants in Croatia resulted in high particle number concentrations of 1×10^{7} to 3×10^{10} particles/g. The scanning electron microscopy coupled with energy dispersive X-ray spectroscopy (SEM-EDS) providing insights into the origin of the particles and their transformation pathways. The risk assessment concluded that there are negligible to low ecological risks under current agricultural application scenarios, although potential negative impacts should be assessed in long-term projections. The methodology presented in this work addresses critical gaps in environmental monitoring capabilities for engineered NPs in their primary environmental sink.

Keywords: Metallic nanoparticle; Single-particle ICP-MS; Sewage sludge; Extraction optimization; Environmental risk assessment

Environmental Implication

Metal- and metal oxide-based engineered nanoparticles (NPs) are a growing environmental concern due to their increasing use and inevitable release into the environment. We present an optimized analytical approach that enabled a comprehensive analysis of seven metallic NPs, including the first-time quantification of PbO NPs in solid environmentally matrices. The developed analytical method opens up avenues for the routine analysis of metallic NPs, addressing a critical gap in environmental monitoring capabilities and providing essential data for more accurate risk assessments and evidence-based regulatory decisions.

1. Introduction

Nowadays, the human population is exposed to an increasing number of chemical pollutants. Metal- and metal oxide-based engineered nanoparticles (NPs) represent an important group of so-called

"*emerging contaminants*" due to their small size (1–100 nm) and high surface reactivity, which enable them to penetrate biological cell walls and membranes (El-Kalliny et al. 2023; Keller et al. 2017). Given their wide array of applications in technology development and manufacturing, metallic NPs (MNPs) emissions into the environment are inevitably on the rise, posing increasing risks to living organisms and human health (Abbas et al. 2020; Besha et al. 2020; Yang et al. 2017). While exposure models are considered essential tools for predicting environmental concentrations of MNPs in regulatory risk assessment processes, these models are inherently prone to generalization. Reliable risk assessments require temporally and spatially resolved analytical data on the concentrations and composition of MNPs in the environment (Keller et al. 2024; Nowack, 2017).

Current research indicates that approximately 95% of MNPs ultimately reach wastewater treatment systems after use (Westerhoff et al. 2011). Throughout the wastewater treatment process, these NPs predominantly partition into sewage sludge rather than remaining in the effluent water. This concentration mechanism creates a critical environmental reservoir for MNPs. The subsequent application of this sludge to agricultural soils—a practice that accounts for approximately 31% of sewage sludge management in EU Member States (Eurostat, 2022) and USA (U.S. Environmental Protection Agency, 2023)—establishes a direct pathway for MNPs to enter food production systems and potentially impact human health. While Council Directive 86/278/EEC established limits for conventional heavy metals in sludge-amended agricultural soils, this framework predates our understanding of NP behavior and does not consider the unique properties of MNPs. Unlike their bulk counterparts, nanoparticulate forms exhibit enhanced bioavailability, greater mobility in soil systems, and potentially higher toxicity due to their increased surface area and reactivity (Keller et al. 2017; Ng et al. 2018; Rippner et al. 2021; Wu et al. 2019), properties that make their environmental fate particularly challenging to predict.

The regulatory and environmental concerns are further complicated by significant methodological barriers that hamper accurate quantification and characterization of NPs in complex environmental matrices. These challenges include: (i) extremely low environmental concentrations (i.e., ng L^{-1}) against a complex background of natural particles, dissolved species, and organic matter; (II) transformation processes that alter the physicochemical properties of MNPs during their environmental lifecycle, requiring analytical methods capable of capturing these changes; (III) and lack of standardized protocols for extraction and analysis, resulting in data incomparability across

studies and hindering systematic risk assessment (Abbas et al. 2024; Bundschuh et al. 2018). While electron and atomic microscopy techniques (TEM, SEM, AFM) provide valuable morphological information, their laborious sample preparation requirements limit applicability for routine environmental monitoring. Single-particle inductively coupled plasma mass spectrometry (sp-ICP-MS) has emerged as a promising analytical approach due to its ability to perform sensitive and selective high-throughput measurements with relatively simple sample preparation while simultaneously providing information on number-based particle size distributions and particle mass/number concentrations (Goodman et al. 2025; Laborda et al. 2014; Vidmar et al. 2017).

The validation of analytical methods for NPs in complex matrices using sp-ICP-MS presents unique challenges not encountered with conventional dissolved metal analysis. In contrast to traditional analytes, NPs can undergo multiple transformations during extraction procedures, including dissolution, agglomeration, and even new particle formation (Borowska and Jankowski, 2023; Laycock et al. 2022). These transformations significantly impact the measured particle size distributions, number concentrations, and mass concentrations, often leading to quantitative results that do not accurately reflect the actual NP content in environmental samples. For the quantitative determination of MNPs in environmental samples, several key methodological considerations emerge as critical. No single metric (particle number, mass concentration, or size distribution) provides a complete picture of NPs properties, and thus, truly robust methods must evaluate all relevant metrics, as these parameters have no predictive power for each other. For example, particle aggregation decreases their number concentration and increases the mean particle size, while the mass concentration should remain unchanged. Conversely, dissolution reduces all three measurands, but in different proportions (Laycock et al. 2022). Unlike conventional analytes, where spike recovery of 100 ± 10% is typically acceptable, NP recoveries are more challenging to interpret, necessitating a wider acceptable recovery range of ±25%. This broader range is necessary due to cumulative errors in recovery metrics (Baur et al. 2020; Gray et al. 2013; Laycock et al. 2022).

Several extraction solutions have been employed to extract metallic NPs from complex environmental matrices, including tetrasodium pyrophosphate (TSPP), sodium chloride (NaCl), tetramethylammonium hydroxide (TMAH), various surfactants, and ultrapure water, followed by physical separation techniques such as centrifugation, sedimentation, or filtration (Baur et al. 2020; Moreno-Martín et al. 2022; Schwertfeger et al. 2017; Tou et al. 2021; Vidmar et al. 2022). However,

111 comprehensive comparisons of extraction methodologies across multiple NP types and extraction
112 solutions have been lacking, with previous studies typically focusing on individual extraction methods
113 or specific NP types.

114 This study aims to develop and optimize an extraction and analysis method for seven environmentally
115 relevant MNPs (Ag, Au, CeO_2, CuO, PbO, TiO_2 and ZnO) from sewage sludge. By systematically
116 evaluating extraction efficiency using various solutions (including TSPP and TMAH at different
117 concentrations, and milli-Q water) and optimizing methodological parameters such as settling time
118 and sludge-to-reagent ratios, we aim to establish a standardized protocol for reliable quantification
119 and size characterization of these NPs. This integrated analysis approach overcomes previous
120 knowledge gaps regarding the comparative efficiency of different extraction solutions and provides a
121 more comprehensive assessment of all relevant particle metrics.

122 The optimized method is then applied to analyze sludge samples from five Croatian wastewater
123 treatment plants (WWTPs), providing valuable data on the occurrence and characteristics of these
124 MNPs in real environmental samples. The quantitative assessment of NPs in sludge samples using
125 the sp-ICP-MS method is complemented by structural and chemical characterization by scanning
126 electron microscopy (SEM) coupled with energy-dispersive X-ray spectroscopy (EDS), which reveals
127 critical insights into the chemical speciation and transformation of MNPs in sewage sludge. Finally, we
128 provide an environmental risk assessment using literature toxicity data for the terrestrial environment,
129 classifying risk levels for each MNP under the current scenario. This comprehensive approach makes
130 it possible to close gaps in current analytical approaches and knowledge of real environmental
131 concentrations of MNPs.

132 **2. Material and methods**

133 **2.1 Sample collection**

134 Sewage sludge samples were collected from five municipal WWTPs in Croatia. Sludge from the
135 Zagreb (ZG) WWTP was used for method optimization, after which the optimized protocol was applied
136 to screen for MNPs in samples from WWTPs in Velika Gorica (VG), Čakovec (CAK), Karlovac (KAR),
137 and Sisak (SIS) (Table A1). Following collection, samples were transported to the laboratory, where
138 they were air-dried and sieved through a 2-mm mesh.

2.2. Chemicals

Milli-Q water (18.2 MΩ·cm) from Millipore (Bedford, MA, USA) was used to prepare all solutions. Ionic Ag, Au, Ce, Cu, Pb, Ti and Zn standard solutions for ICP-MS (1000 mg L^{-1}) purchased from Merck (Darmstadt, Germany) were utilized to establish the calibration curves for ICP-MS. Nitric acid (65%) from Kemika (Zagreb, Croatia), hydrochloric acid (37%) from Rotipuran (Karlsruhe, Germany), hydrofluoric acid (47-51%) and boric acid (40 g L^{-1}) from Fluka (Charlotte, NC, USA) were used for the digestion of sewage sludge samples. Tetrasodium pyrophosphate decahydrate (TSPP, purity 99.8%) and tetramethylammonium hydroxide (TMAH, 25%) were procured from Sigma Aldrich (St. Louis, MO, USA) and used as the extraction reagents. Commercial sodium citrate-stabilized (2 mM) gold nanoparticles with a particle diameter of 52 ± 5 nm (as determined by TEM) and Au mass concentration of 0.053 mg mL^{-1} (as determined by ICP-MS), as well as silver nanoparticles with a particle diameter of 40 ± 4 nm (as determined by TEM) and Ag mass concentration of 0.020 mg mL^{-1} (as determined by ICP-MS) were obtained from NanoComposix (San Diego, CA, USA). These nanoparticle suspensions were employed to prepare Au and Ag NP standard working solutions and spiked sewage sludge samples. For the spiking experiments, aqueous suspensions of CeO_2 NPs (30-50 nm) and CuO NPs (25-55 nm), each containing 20 wt% of the respective NPs, were purchased from US Research Nanomaterials (Houston, TX, USA), while TiO_2 nanoparticle standard reference material (SRM 1898) was obtained as s powder from NIST (Gaithersburg, MD, USA). According to the certificate of analysis provided by NIST, SRM 1898 consists of 76% anatase and 24% rutile, with TiO_2 particles of a primary size < 50 nm (as observed by TEM) and a volume-weighted mean diameter of 71 nm in a water suspension, as determined by laser diffraction spectrometry (LDS). Lead (II) oxide (PbO) and zinc oxide (ZnO) NPs were synthesized as powders by means of a sol-gel method and by employing gelatine as stabilizer. The synthesized particles exhibited diameters of 250 nm for PbO NPs and 30 nm for ZnO NPs (Figure A1-A3). Details of the synthesis process of PbO and ZnO NPs can be found in Appendix A. For PbO and ZnO synthesis, the lead (II) nitrate and zinc nitrate hydrate, as well as gelatine were obtained from Sigma Aldrich (St. Louis, MO, USA).

2.3. Physicochemical characterization and multielement analysis of sludge samples

Particle size analysis of sludge samples was performed using a laser-based particle size analyzer (LS 13320, Beckman Coulter Inc.) The particle size distribution (PSD) was calculated on the basis of the

Mie theory of light scattering (optical parameters: refractive index = 1.53; absorption index = 0.1). Prior to analysis, the samples were treated with 2.5 mM TSPP solution to avoid flocculation. Organic matter (OM) content was estimated using the loss on ignition (LOI) method (Salehi et al. 2011). LOI was determined gravimetrically after dry ashing at 360°C over 2 h.

For multielement analysis, the samples were digested in a microwave oven (Multiwave 3000, Anton Paar, Graz, Austria) in a two-step total digestion procedure (I step: 5 mL HNO_3 (65% p.a.) + 1 mL HCl (36% s.p.) + 1 mL HF (48% s.p.), and II step: 6 mL H_3BO_3 (40 g L^{-1})). The analysis was performed using an inductively coupled plasma triple quadrupole mass spectrometer (ICP-MS/MS, 8900, Agilent Technologies, USA). Analytical quality control was ensured through simultaneous analysis of procedural blanks and certified reference materials (Soil NCS DC 773902, GBW 7410; China National Analysis Centre for Iron and Steel, Beijing, China). Good recoveries (90–100%) were obtained for all measured elements.

2.4. Optimization of nanoparticle extraction from sewage sludge

To optimize the nanoparticle extraction method for sludge samples, spike suspensions containing Ag, Au, CeO_2, CuO, PbO, TiO_2 and ZnO NPs were prepared. Most spike solutions of NPs supplied as aqueous suspensions were prepared by bath sonication in milli-Q water for 10 min, with the exception of Ag NPs, which achieved optimal stability in 2 mM trisodium citrate. TiO_2 and ZnO powders were dispersed directly in milli-Q water, while PbO NP powder was dispersed in Moringa Oleifera (MO) extract to obtain 1 mg mL^{-1} NP suspensions. The MO extract was prepared by shaking 5 mg of MO powder in 20 mL of milli-Q water for 3 hours and then filtered through a 0.45 µm filter. Suspensions of NPs were then subjected to probe sonication using a Qsonica Sonicator Q125 (L.L.C, Newton, CT, USA), equipped with a 6 mm probe (model CL-18), and operated at 80 % amplitude in pulse mode. Sonication times were optimized for each material: 8 minutes 48 seconds for TiO_2, 18 minutes for PbO and 12 minutes for ZnO NPs. Since the probe can be a source of TiO_2 NPs, a blank sample (milli-Q water) was sonicated under the same conditions as the TiO_2 NPs suspension. The concentration of TiO_2 NPs detected in the blank was then subtracted from the concentrations measured in the actual samples. During the entire sonication, the vials were placed in an ice bath to prevent the suspension from overheating. Since PbO NPs showed dissolution behavior at high

196 dilutions, the stability of the spike solution was maintained by adding stock solution to 50 mg MO
197 powder and shaking throughout the extraction process, which ensured excellent stability of the
198 suspension. The optimization of the extractions was performed at least in duplicate, while the final
199 validation was conducted in quintuplicate. Sludge samples (0.20 g each) were weighed into
200 polypropylene tubes and combined with 20 mL of extraction solution. Nanoparticle spike suspensions
201 were added to achieve specific concentrations as follows: 40 µg g^{-1} for Ag, Au, and Ce; 100 µg g^{-1} for
202 Cu; and 1000 µg g^{-1} for Ti, Pb, and Zn. The volumes and concentrations of the added NP
203 suspensions were: Au (151 µL of 0.053 mg mL^{-1}), Ag (400 µL of 0.020 mg mL^{-1}), CeO_2 (40 µL of 0.20
204 mg mL^{-1}), CuO (100 µL of 0.20 mg mL^{-1}), PbO (200 µL of 1 mg mL^{-1}), TiO_2 (200 µL of 0.10 mg mL^{-1}),
205 and ZnO (200 µL of 1 mg mL^{-1}). These concentrations were selected to approximately match the
206 levels of respective elements found in sludge from the Zagreb WWTP that was used for method
207 optimization. After the 24 h incubation, the samples were shaken for 24 h at 300 rpm on an orbital
208 shaker (Edmund Bühler GmbH, Germany) and subsequently sonicated for 20 min in a sonication
209 water bath (Iskra PIO, Šentjernej, Slovenia). In this experiment, the probe sonication was also tested
210 for the nanoparticle extraction from sludge samples and resulted in a significantly higher number of
211 recovered NPs (results not shown), which is consistent with previous studies (Bland and Lowry, 2020;
212 Schwertfeger et al. 2017; Tou et al. 2021). However, since the probe can be a source of TiO_2 NPs, its
213 further use was omitted in the development of the method.

214 The second step in optimizing the extraction efficiency was to calculate the settling time for NP
215 separation from the liquid phase, which mainly depends on the viscosity of the extractant and the
216 particle density. A particle size threshold of 450 nm was established for nanoparticles spiked to
217 sludge, assuming a particle density of 15 g cm^{-3}. The particle density of 15 g cm^{-3} was selected after
218 the testing, as the optimal compromise for simultaneous multielement analysis across a range of
219 particle densities, from TiO_2 NPs (3.92 g cm^{-3}; considering mostly anatase composition) to Au NPs
220 (19.3 g cm^{-3}). Based on Stokes' law, the estimated time was calculated using different solution
221 viscosities and then an aliquot was taken from the upper liquid layer (0.1−0.5 cm deep) of the
222 extracted sample for analysis. The effect of different sludge-to-reagent ratios, namely 1:100 (200 mg
223 sludge and 20 mL solution) and 1:1000 (20 mg sludge and 20 mL solution), on the recovery of the
224 particle was also tested.

In the third step of optimization, the different extraction media were examined for their capacity to extract nanoparticles and, at the same time, limit the dissolution and agglomeration of the particles. The solutions tested in these experiments include: 1) mili-Q water, which is the mildest extraction solution and can extract the particles readily mobilized in the sludge; 2) TMAH at various concentrations of 5%, 10%, 15%, 20%, and 25%; and 3) TSPP at various concentrations of 2.5 mM, 10 mM, and 20 mM. Details on the extraction procedures performed when using different extraction solutions can be found in Table A2.

2.5. Sp-ICP-MS measurements

Sp-ICP-MS measurements were performed on a model 7900 ICP-MS instrument from Agilent Technologies (Santa Clara, CA, USA) equipped with a quadrupole mass analyser. The operating parameters (summarized in Table A3) were optimized for plasma robustness and sufficient sensitivity. Silver, Au, Ce, Cu and Pb in aqueous standard solutions were analysed for their most abundant isotopes ^{107}Ag (51.84%), ^{197}Au (100%), ^{140}Ce (88.4%), ^{63}Cu (69.2%) and ^{208}Pb (52.4%), while Ti and Zn were measured at ^{47}Ti (7.3%) and ^{66}Zn (27.7%) to minimize isobaric interferences from ^{48}Ca to ^{48}Ti and ^{64}Ni to ^{64}Zn, but also polyatomic interferences from sulphur and nitrogen. Silver, Au, Ce, Pb and Ti were analysed in no gas mode, while Cu and Zn were analysed in helium collision mode (4.3 mL min^{-1} He gas flow).

The measurements were run in the time-resolved-analysis (TRA) mode in order to collect the intensity for a single particle as it is vaporized and ionized in the plasma. A short integration dwell time of 100 µs per reading was set. An accurate sample flow rate (at peristaltic pump speed of 0.1 rotations/s) was determined daily by pumping a known weight of milli-Q water at room temperature (N=3). The transport efficiency was determined according to the “particle size” method (Pace et al. 2011) from a suspension of 53 nm gold nanoparticles (nanoComposix, San Diego, CA, USA) of known concentration (0.05 mg mL^{-1}). The suspension was appropriately diluted with milli-Q water to reach an Au NP concentration of 132 ng L^{-1}. For calibration, a series of dissolved Au standards (0, 0.1, 0.5, 1, 5 and 10 µg L^{-1}) were prepared from a stock standard solution of ionic Au (1000 mg L^{-1}) in 2% (v/v) HCl/0.5% w/v Thiourea solution (Inorganic ventures, Christiansburg, VA, USA) in milli-Q water. For all samples, the dilution factor was adjusted in such a way that the number of detected particles during 1 min acquisition was >100 to reduce the random error governed by Poisson statistics to 10% and lower

than 3800 to limit relative bias due to multiple particle events to below 3%, assuming a transport efficiency of 0.11 (11%), sample flow rate of 0.33 mL/min, and a dwell time of 100 µs.

2.6. Data treatment

The raw signal intensity data from ICP-MS were processed using spCal software (Lockwood et al. 2021). SpCal is an open-source Python-based sp-ICP-MS data processing platform with an interactive graphical user interface, enabling the large data sets to be analysed using transparent algorithms. For our purpose, the Poisson-based data filtering (α=0.01) was used to differentiate particle signals from background noise.

To calculate particle size, the particle mass was converted to diameter assuming spherical geometry with specific mass fractions and densities (Table A4). While PbO NPs possess a plate-like structure, the spherical approximation was employed to simplify calculations without compromising the accuracy of recovery determinations. Nanoparticle recovery was evaluated using multiple metrics for comprehensive characterization (see Appendix B for details). The mean particle diameter recovery (R_{MD}) was calculated as follows:

$$R_{MD}\,(\%) = \frac{C_{SS}}{C_S} \times 100 \quad (1)$$

Where C_{SS} is the mean diameter of particles detected in the spiked sewage sludge samples, and C_S is the mean diameter of particle in the spike solution prepared in mili-Q water (or in MO extract in the case of PbO). The three additional recovery metrics, including particle number concentration recovery and two mass recovery metrics (particle mass and total mass recoveries), were calculated using the following equation:

$$R_M\,(\%) = \frac{(C_{SS} - C_C)}{C_S} \times 100 \quad (2)$$

Where C_{SS} is the concentration of the relevant metric (number of particles, particle mass, and total mass of element) in the spiked sewage sludge samples, C_C is the concentration of the same metric in the (non-spiked) control sludge sample, and C_S is the concentration of the same metric in the spike solution. Total mass recovery is based on the mean signal value of the time-resolved analysis data

over the specified range and represents the sum of particulate and ionic mass recovery. The graphs were created in the R platform (R Core Team 2023).

2.7. Electron microscope analysis

The supernatants were obtained from the sludge extracts, which were shaken with milli-Q water for 24 h. One or two drops of the supernatants were then analyzed for structural (morphological) and chemical composition using scanning electron microscopy (SEM, Verios G4 HP) and energy dispersive X-ray spectroscopy (EDXS, Ultim Max SDD 65 mm^2). The powder of synthesized PbO and ZnO NPs was also analyzed to determine size and morphology.

3. Results and discussion

3.1. Physico-chemical characterization of sewage sludge samples

The physico-chemical characterization of sewage sludge samples from five WWTPs revealed distinctive compositional profiles (Table A5 and A6). The pH values of sludge samples extracted from the Zagreb WWTP exhibited a concentration-dependent response during extraction optimization, with TSPP generating a wide range of pH conditions (pH 6.68-9.55) while all TMAH concentrations produced strongly alkaline environments (pH >13). Considering other WWTPs, the pH values showed slight variation within the mildly acidic to neutral range, from 6.33 (CAK) to 6.88 (SIS). Particle size analysis demonstrated that silt was the predominant fraction across all samples, ranging from 57.94% to 86.34%, with SIS containing the highest proportion and CAK the lowest. Sand content exhibited substantial variation, with CAK having the highest percentage (35.11%) and SIS the lowest (3.58%). Clay content ranged from 4.73% in KAR to 15.21% in VG. When analyzing the particle number, the smallest particles dominate, with over 80% of the total particle count falling within the 40-160 nm range. The primary mode across all samples is 80 nm (Fig. A4). The organic matter (OM) content varied considerably between 470 mg g^{-1} (SIS) and 811 mg g^{-1} (VG), indicating significant organic enrichment in all sludges. Total metal concentrations revealed notable variations across samples (Table A7), with SIS containing the highest concentrations of Al (25.1 mg g^{-1}), Ba (389 µg g^{-1}), Mg (9.99 mg g^{-1}), Na (2.61 mg g^{-1}), Ti (2.10 mg g^{-1}), and Ce (28.1 µg g^{-1}). ZG exhibited the highest levels of Ca (43.8 mg g^{-1}), Ag (3.21 µg g^{-1}), Cu (323 µg g^{-1}), and Pb (1.09 mg g^{-1}), while CAK contained the highest concentrations of Fe (27.4 mg g^{-1}), K (8.97 mg g^{-1}), P (29.2 mg g^{-1}), and Zn (1.17 mg g^{-1}).

Comparison with regulatory standards revealed that all metal concentrations were below the Croatian permissible levels for processed sludges used in agriculture (Cu: 600 μg g^{-1}, Pb: 500 μg g^{-1}, Zn: 2,000 μg g^{-1}), except for Pb in ZG (1,090 μg g^{-1}), which exceeded the Croatian standard, while remaining within the EU Directive 86/278/EEC upper range (750–1,200 μg g^{-1}).

3.2. Optimization and evaluation of extraction efficiency for nanoparticles in sewage sludge

By systematically evaluating the extraction efficiency of nanoparticles from sludge samples—taking into account their size, particle number, and mass concentration—several key parameters were optimized, including the sludge-to-reagent ratio, type and concentration of the extraction media, and the settling time needed to separate the extracted nanoparticles from the residual matrix.

First, the optimal sludge-to-reagent ratios (1:100 and 1:1000) were systematically evaluated for NP recovery using TMAH (5% and 25%) as an extraction solution. In these preliminary experiments, NPs with varying densities (TiO_2, CeO_2, and Au NPs) were tested. The results showed minimal differences in NP recoveries between the two tested ratios, with the 1:100 ratio providing slightly better extraction efficiency while preventing sample swamping and enhancing spike incorporation into the sludge matrix (Table A8). Based on these findings and subsequent comparative experiments with TSPP, we found that the 1:100 ratio ensures optimal performance for the targeted NPs in method development experiments.

Following extraction and before sp-ICP-MS analysis, nanoparticles must be separated from the residual matrix to avoid clogging the nebulizer with larger sludge particles. Several papers have highlighted the importance of settling particles to maximize the recovery of spiked NPs from solid matrices, as centrifugation can lead to the loss of heavier particles when working with nanoparticles of different densities (Liu et al. 2021; Moreno-Martín et al. 2022; Tou et al. 2021). Based on Stokes' law, the settling time was calculated for particles with a diameter of 450 nm in solutions of varying viscosities (Table A2). For TSPP and milli-Q water, the settling time was set at 2 h and 30 min due to their similar viscosities. For TMAH solutions, the settling times increased with concentration: 3 h and 20 min for 5% TMAH, 4 h and 10 min for 10% TMAH, 5 h and 10 min for 15% TMAH, 6 h and 10 min for 20% TMAH, and 7 h and 20 min for 25% TMAH.

Despite the growing concern about ENPs in the environment, a comprehensive comparison of extraction methodologies across multiple nanoparticle types and extraction solutions has been lacking. Previous studies have typically focused on individual extraction methods or specific metallic NPs, leaving significant knowledge gaps regarding the comparative efficiency of different extraction solutions and the simultaneous assessment of all relevant particle metrics (number recovery, mass recovery, total recovery and diameter changes). The following section of this paper will discuss the recoveries and behavior of seven MNPs across different extraction solutions (milli-Q water, TSPP and TMAH), providing a more integrated analysis than previously available. For partially soluble NPs such as Ag NPs, CuO NPs, and ZnO NPs, extraction methods were evaluated both with and without of 24 h incubation period. These conditions allowed us to assess the impact of temporal factors on nanoparticle stability and recovery efficiency in complex sludge matrix.

Gold nanoparticles. For Au NPs, TSPP at different concentrations emerged as the optimal extraction solution, with the 20 mM concentration showing the best performance across multiple recovery parameters (Fig. 1; Table A9). The TSPP maintained the integrity of the Au NPs with minimal change in their size (mean diameter 100 ± 1.4%) while achieving high NP number recovery (for 20 mM TSPP: 89.5 ± 8.5%) and good mass recovery metrics (NP mass recovery: 93.5 ± 7.4%; total mass recovery: 92.8 ± 8.2%). In contrast, TMAH performed poorly, especially at lower concentrations (5%), with a remarkably low NP number recovery (1.3 ± 70.5%) accompanied by significant size alterations (mean diameter recovery 137.8 ± 3.6%). Increasing TMAH concentration to 25% improved recovery but still resulted in substantial particle size changes. A number of studies have raised concerns about particle agglomeration in the presence of TMAH in biological samples, which could potentially lead to particle loss (Laycock et al. 2022). Since TMAH causes strongly alkaline conditions with pH values above 13.0 (Table A5), it can cause solubilization of various organic compounds in the sludge matrix, including humic substances, proteins and polysaccharides, by deprotonation of organic functional groups (Li et al. 2016). This solubilization process can destabilize the electric double layer surrounding Au NPs, which affects the surface charge of the nanoparticles and the aggregation behavior in the aquatic environment. Diegoli et al. (2008) specifically found that high ionic strength conditions can cause charge screening, creating "bridges" between Au NPs and thereby facilitating their aggregation. The observed concentration-dependent recovery of Au NPs with TMAH (mass recovery; 8.0 % at 5 % TMAH vs. 74.6 % at 25 % TMAH)

should be further investigated beyond the scope of this study. Future research should specifically examine the mechanisms behind this counterintuitive behavior, possibly exploring the interplay between the partial or complete solubilization of organic matter and the changing ionic strength environment at different TMAH concentrations. Milli-Q water demonstrated moderate extraction ability (NP number recovery: 57.0 ± 5.9%; NP mass recovery: 83.8 ± 12.6%); however, TSPP significantly outperformed it in NP number recovery, achieving almost 30% higher efficiency.

Silver nanoparticles. Ag NPs exhibited distinct behavior in extraction studies (Fig. 1; Table A10). Notably, 24 h incubation resulted in significant dissolution and diminished recoveries across all extractants (e.g., 2.5 mM TSPP yielded only 67.5 ± 4.3% size recovery, 35.2 ± 16.6% number recovery, and merely 13.4 ± 8.6% mass recovery). This pronounced degradation is likely due to complex sludge interactions in which humic acids and ammonia form soluble Ag $(NH_3)_2$+ complexes, while chloride ions produce $AgCl_2$ and $AgCl_{(aq)}$ species (Jiang et al. 2022), with these reactions occurring despite pH conditions that would normally reduce dissolution. To circumvent these dissolution challenges, we modified our protocol to eliminate the incubation period and prevented the time-dependent dissolution processes that would otherwise occur. Under these optimized conditions, TSPP at varying concentrations (2.5, 10, and 20 mM) demonstrated excellent performance metrics: number recoveries of 96.5 ± 6.8%, 100.7 ± 3.0%, and 108.2 ± 3.6%, respectively, with corresponding mass recoveries of 107.4 ± 6.7%, 109.3 ± 2.5%, and 116.4 ± 3.0%. Moreover, milli-Q water also performs well under these specific conditions, providing high recovery rates (102.8 ± 0.2% size recovery, 96.3 ± 1.7% number recovery, 108.8 ± 0.3% mass recovery). Interestingly, the sludge matrix with extraction solution provided additional stabilization of Ag NPs compared to spike solutions in 2 mM trisodium citrate, explaining the slightly increased but acceptable mass recoveries. TMAH extractant exhibited clear concentration dependence: lower TMAH concentrations (5-10%) maintained satisfactory number recovery (117.3 ± 0.5% and 105.8 ± 1.6%) despite elevated mass recovery (130.5 ± 3.3% and 155.0 ± 3.1%), while higher TMAH concentrations (15-25%) dramatically reduced recovery efficiency (declining to 45.6 ± 25.5% at 15%) due to pronounced Ag NP aggregation. These findings emphasize the critical importance of controlling both sample aging and extraction conditions when analyzing Ag NPs in high-organic environmental matrices, as the time-dependent transformation processes significantly impact nanoparticle recovery and characterization results.

Cerium nanoparticles. TSPP performed well with consistent and favorable performance for CeO_2 NPs (Fig. 1; Table A11). At 2.5 mM concentration, NP number recovery reached 90.6 ± 9.1%, with moderate mass recovery metrics (NP mass recovery: 75.7 ± 4.8%; total mass recovery: 100.0 ± 10.2%). TSPP extraction resulted in a slight reduction in mean particle diameter (94.8 ± 2.2%), suggesting minimal transformation of analyzed particles. Higher TSPP concentrations (10 and 20 mM) showed similar effectiveness in number recovery (91.4 ± 6.3% and 92.4 ± 5.7% respectively) with comparable size changes, indicating that CeO_2 NPs respond consistently to TSPP extraction regardless of concentration within the tested range. TMAH extraction presented an interesting pattern across its concentration gradient. All TMAH concentrations (5-25%) demonstrated high NP number recovery, ranging from 105.5 ± 0.5% at 5% TMAH to 125.3 ± 5.5% at 20% TMAH, while mass recovery remained satisfactory (78.8 ± 6.0% to 90.0 ± 11.2%) and increased proportionally with TMAH concentration. Milli-Q water showed moderate effectiveness for CeO_2 NP extraction, with number recovery at 52.4 ± 2.2% and mass recovery at 74.0 ± 8.0%. However, milli-Q water caused an increase in mean particle diameter (113.5 ± 0.6%), suggesting potential agglomeration into the larger particles. The substantial size alteration coupled with moderate recovery indicates that water alone is insufficient for optimal CeO_2 NP recovery from sludge due to its limited ability to disperse organic matter and disrupt metal-organic bridges.

Copper nanoparticles. 2.5 mM TSPP demonstrated excellent nanoparticle number recovery both with incubation (93.3 ± 8.0%) and without incubation (93.7 ± 3.9%), making it the most effective extraction solution for CuO NPs (Fig. 1; Table A12). However, this high recovery was accompanied by a reduction in mean particle diameter (85.9 ± 3.6% with incubation; 84.5 ± 0.5% without incubation) and variable mass recovery (72.9 ± 25.0% with incubation; 82.2 ± 1.2% without incubation), with immediate extraction yielding more consistent mass recovery. To investigate the potential aggregation of the CuO NPs in the spike solution, which can lead to smaller diameters in the sludge samples (Cervantes-Avilés et al. 2021), we also tested the spike solution prepared in an isolated dissolved sludge matrix. The results remained consistent with 87.1 ± 4.7% of mean particle recovery, excluding aggregation as a contributing factor. Higher TSPP concentrations (10 and 20 mM) showed concentration-dependent effects that varied with incubation time. Without incubation, 20 mM TSPP yielded higher performance (NP number: 91.3 ± 4.2%; mass recovery: 76.1 ± 0.4%) compared to the 24 h incubation results (NP number: 65.9 ± 5.3%; mass recovery: 65.3 ± 9.7%), suggesting that

prolonged exposure in sludge media may promote dissolution. In contrast, TMAH performed poorly for NP number recovery, with effectiveness declining sharply as concentration increased (from 37.3 ± 0.5% at 5% TMAH to 23.8 ± 15.2% at 25% TMAH). Interestingly, TMAH showed poor recovery of particle number but satisfactory recovery of mass (from 100.3 ± 0.5 % at 5 % TMAH to 70.3 ± 12.2 % at 25 % TMAH) and higher recovery of mean diameter (from 102.4 ± 12.4 % at 10 % TMAH to 111.8 ± 1.6 % at 15 % TMAH), suggesting aggregation of CuO NPs under alkaline conditions. Milli-Q water demonstrated limited extraction capability with incubation (NP number recovery: 39.8 ± 10.3%; mass recovery: 61.4 ± 20.7%) but showed slightly better performance for mass recovery without incubation (71.9 ± 21.1%).

Lead nanoparticles. For PbO NPs, extraction with milli-Q water alone yielded moderate NP number (71.9 ± 16.2%) and mass (73.1 ± 22.1%) recoveries (Fig. 1; Table A14), with relatively low total mass recovery (44.1 ± 14.7%) and a constant particle size (103.5 ± 0.7%). In comparison, 2.5 mM TSPP exhibited the most balanced performance among all tested solutions. It achieved good recovery of NP mass (84.1 ± 14.3%) alongside moderate recovery of number (76.5 ± 8.7%), while maintaining acceptable recovery of particle size (105.6 ± 0.6%) and total mass (80.6 ± 8.9%). Higher TSPP concentrations showed diminished performance for nanoparticle-specific metrics; 10 mM TSPP resulted in moderate NP mass recovery (52.2 ± 0.2%) and lower number recovery (49.8 ± 7.9%), while 20 mM TSPP yielded poor results for both NP number (37.8 ± 13.9%) and mass (38.2 ± 13.7%). Notably, total mass recovery increased substantially with higher TSPP concentrations, reaching 220.9 ± 14.5% at 20 mM, suggesting increasing interaction with the sludge matrix at higher pH values of 9.55 (Table A5). TMAH exhibited highly anomalous behavior across all tested concentrations (5%, 10%, and 25%), with recovery values frequently exceeding 100%, particularly for mass recovery metrics (e.g., 5% TMAH: NP mass 277.1 ± 13.8%, total mass 793.9 ± 5.0%; 25% TMAH: NP mass 448.3 ± 2.7%, total mass 1858.2 ± 1.7%). The extraordinarily high total mass recovery, especially with 25% TMAH, strongly suggests solubilization of background lead from the sludge matrix itself and the formation of soluble hydroxide complexes, where the alkaline conditions not only mobilize the added Pb spikes but also dissolve naturally occurring Pb within the sludge, causing concentrations to increase disproportionally in spiked samples compared to control sludge samples (Zeng et al. 2017; Pranudta et al. 2021).

Titanium nanoparticles. Titanium dioxide NPs exhibited specific recovery patterns for the different extractants with different behaviors in mean size, number and mass of recovery metrics (Fig. 1; Table A13). The mean size recovery was consistently above 100 % for most extraction methods, indicating possible agglomeration effects, with TSPP extractions yielding 107.5 ± 2.0 % at 2.5 mM and peaking at 112.3 ± 1.2 % at 10 mM. TMAH demonstrated a concentration-dependent trend in size recovery, starting at 97.2 ± 2.0% (5% TMAH) and increasing to 111.4 ± 9.0% at 25% concentration. For particle number recovery, TSPP consistently provided the best results, with optimal recovery at 10 mM (99.6 ± 3.4%), while TMAH showed significant variability, performing best at 15% concentration (81.1 ± 7.1%) but declining sharply at both 10% (61.1 ± 11.9%) and 25% (59.8 ± 32.6%). Mass recovery patterns revealed complex dynamics, with mili-Q water producing unusually high recovery (118.3 ± 2.6%), TSPP showing a concentration-dependent increase from 90.4 ± 11.6% to 108.3 ± 1.1%, and TMAH demonstrating the most variable results with a pronounced minimum at 10% concentration (48.3 ± 0.6%). Overall, these results indicate that the extraction efficiency of TiO_2 NPs is highly dependent on both extractant type and concentration, with an inverse relationship observed in certain cases between particle number and size/mass recovery. This phenomenon can be attributed to the strong affinity of TiO_2 NPs for organic matter in complex environmental matrices such as sludge (Wang et al. 2021). Stronger extractants (particularly evident when comparing milli-Q water and TSPP) more effectively disrupt organic-nanoparticle interactions, yielding more accurate number concentration, albeit potentially at the expense of mass recovery efficiency.

Zinc nanoparticles. ZnO NPs presented significant analytical challenges, with limited recovery success across tested extraction methods, thus only results of milder solutions are reported (Table A15). Both milli-Q water and 2.5 mM TSPP extractions yielded poor recoveries, with no improvement observed in non-incubated samples (results not shown). These extraction methods resulted in substantial particle size reduction (mean diameter 64.4 ± 5.7% for milli-Q water and 63.4 ± 0.7% for 2.5 mM TSPP), indicating immediate dissolution and transformation during the extraction process. Nanoparticle number recovery was markedly deficient for both methods, with milli-Q water achieving only 34.4 ± 3.0% recovery and 2.5 mM TSPP yielding 42.0 ± 25.8% recovery with high variability. Even worse were the extremely low mass recovery metrics, with NP mass recoveries of merely 5.0 ± 15.0% and 6.9 ± 28.7%, while total mass recoveries reached only 21.2 ± 36.8% and 0.4 ± 17.8% for milli-Q water and TSPP, respectively. The dramatic size reduction coupled with poor recovery metrics

strongly suggests high reactivity and/or very poor stability, and substantial dissolution of ZnO NPs in the sludge environment, likely due to complexation with abundant organic ligands in the sludge matrix, particularly extracellular polymeric substances and natural organic matter that can bind dissolved Zn^{2+} ions and accelerate nanoparticle transformation (Gomez-Gonzalez et al. 2022). The enhanced dissolution is further facilitated by the increased surface area-to-volume ratio of smaller nanoparticles (approximately 30 nm in diameter), which exhibit greater dissolution compared to larger particles (Mudunkotuwa et al. 2011). Consequently, quantitative results for ZnO NPs should be interpreted with considerable caution, as existing extraction protocols appear inadequate for accurately preserving and recovering these highly reactive NPs from environmental matrices.

Figure 1.

Further recommendations. Based on the comprehensive evaluation of the extraction efficiency of seven NP types (Au, Ag, CeO_2, CuO, TiO_2, PbO and ZnO), 2.5 mM TSPP was finally validated as the optimal extraction solution (Fig. 2). The optimized extraction protocol for stable nanoparticles (i.e., Au, CeO_2, PbO, TiO_2) comprised the treatment of 200 mg of sludge sample with 20 mL of 2.5 mM TSPP solution, corresponding to a sludge-to-reagent ratio of 1:100. The mixture was incubated for 24 h, followed by sonication for 20 minutes to enhance nanoparticle dispersion. Subsequent gravitational settling for 2 h and 30 min allowed separation of the solid matrix and the resulting supernatant was appropriately diluted prior to the analysis of MNPs using sp-ICP-MS. However, for partially soluble nanoparticles (i.e., Ag NPs and CuO NPs), the incubation step was eliminated to preserve nanoparticle integrity. Thus, immediate extraction with 2.5 mM TSPP solution without incubation yielded optimal recovery results, maintaining nanoparticle stability while effectively separating them from the sludge matrix. This procedure consistently demonstrated high performance in particle number (over 75 %) and mass recovery (over 84.5 %), while preserving reasonable particle size consistency throughout (Fig. 2). Based on the consistent high recovery rates across multiple metrics, we recommend 2.5 mM TSPP as a reliable extraction solution for routine analytical procedures involving MNPs in complex environmental samples, particularly when preservation of NP properties is essential for further characterization and quantification.

Figure 2.

3.3. Occurrence and origin of (nano)particles in sewage sludge

The optimized extraction protocol was applied to characterize MNPs in sewage sludge samples collected from five WWTPs in Croatia. This characterization was combined with a geochemical analysis strategy that normalizes observed element concentrations in bulk sludge samples to background levels. The strategy calculates local enrichment factors (EFs; see Appendix A) to assess contamination levels and determine their origin. The EFs revealed distinctive metal accumulation patterns across the five studied WWTPs (Fig. A5). Silver showed notably high enrichment (EFs ~40-250) across all facilities, indicating mainly anthropogenic origin. This was mirrored in NP concentrations (Fig. 3), with Ag NPs being particularly abundant in VG (2.24×10^{8} particles/g; mean diameter of 22.3 nm, Fig. 4) and CAK (1.48×10^{8} particles/g; mean diameter of 20.2 nm). Strong enrichment was observed for Pb in the Zagreb WWTP (EFs ~70-90), corroborated by exceptionally high PbO NP concentrations measured specifically in ZG sludge (2.68×10^{10} particles/g; mean diameter of 25.4 nm), far exceeding other sites. Similarly, Zn and Cu showed significant enrichment (EFs ~9.0-31.5 for Zn; 12.3-35.1 for Cu), with the highest EFs in VG. This correlates well with the NP concentration data, where VG exhibited the highest ZnO concentration (3.25×10^{9} particles/g; mean diameter of 78.0 nm), while CuO NP concentrations were notably elevated across ZG, VG, and CAK ($1.22–1.33\times10^{10}$ particles/g; mean diameter of 40.4–42.8 nm). These findings suggest substantial anthropogenic inputs from the respective catchment areas. In contrast, Ce displayed no enrichment (EFs ~1.0), revealing predominantly natural sources, with CeO_2 NPs being most concentrated in SIS and CAK sludge (2.3×10^{9} and 2.59×10^{9} particles/g; mean diameter of 19.5 and 20.1 nm). Titanium showed slight enrichment (EFs >1.5 for ZG and VG), indicating a partially anthropogenic origin in the bulk sludge (Westerhoff et al. 2015), whereas TiO_2 NP concentrations were highest in VG (8.56×10^{9} particles/g; mean dimeter of 111 nm) and SIS (7.58×10^{9} particles/g; mean dimeter of 99.5 nm).

Figure 3.

The mass concentration of MNPs is consistent with the patterns of particle number concentration and confirms the spatial distribution trends observed across the five Croatian WWTPs (Fig. A6). VG consistently exhibited the highest concentrations for most elements on average (TiO_2: 70.73 µg g^{-1}, ZnO: 8.40 µg g^{-1}, CuO: 5.41 µg g^{-1}, Ag: 0.019 µg g^{-1}, Au: 0.003 µg g^{-1}), indicating a significant anthropogenic input from industrial activities and urban runoff in its catchment area. An exception to

539 this pattern was ZG, which had elevated PbO concentrations (on average 5.00 μg g^{-1}) compared to
540 other sites (0.18-0.77 μg g^{-1}), and SIS, which recorded the highest CeO_2 concentrations (on average
541 0.120 μg g^{-1}), consistent with the natural geological sources indicated by the enrichment factor
542 analysis. When compared to total metal content obtained through acid digestion, extraction efficiency
543 varied across sludge samples (Table A16), with most MNPs representing less than 1% of total metal
544 content for Ag, Ce, Pb, and Zn, while Cu and Ti showed higher percentages (even 4.4% and 10.3%,
545 respectively, at VG). These recovery percentages reflect the limited extractability of MNPs from the
546 sludge matrix, attributed to strong particle-matrix interactions and organic matter complexation (Wang
547 et al. 2021). Additionally, nanoparticle transformation processes during wastewater treatment may
548 further reduce extraction efficiency (Kim et al. 2014).

549 **Figure 4.**

550 *SEM-EDS analysis.* The SEM-EDS provided crucial insights into the composition and
551 transformation pathways of MNPs within the complex matrix of WWTP sludge. While sp-ICP-MS
552 analysis indicated the presence of indigenous Au NPs in some sludge samples (e.g., VG, CAK, and
553 ZG), SEM-EDS analysis confirmed only the presence of spiked Au NPs that were introduced for
554 extraction optimization. Following their introduction, Au NPs primarily interacted with sludge
555 components possibly through surface associations, particularly with sulphur-containing organic matter
556 and Fe-compounds (Fig. A7). Silver particles in the native samples were predominantly present as
557 AgS, as demonstrated by the near-stoichiometric atomic ratios of Ag:S, along with secondary
558 associations of Ca and P in addition to various minor elements (Fig. A8). This indicates that the
559 transformed Ag NPs were likely at least partially amorphous, forming AgS species whose properties
560 (such as higher solubility) differed from the crystalline Ag_2S commonly observed after passage
561 through wastewater systems and treatment plants (Kraas et al. 2017). Cerium-containing particles
562 identified in sludge samples presented a distinctive rare earth element (REE) signature (Fig. A9).
563 SEM-EDS analysis detected a remarkable assemblage of multiple REEs (La, Ce, Pr, Nd, Sm, Gd)
564 alongside thorium and phosphorus - a composition strongly indicative of monazite or processed REE-
565 phosphate materials (Dar et al. 2025). These REE-phosphate particles showed minimal
566 transformation during anaerobic digestion, maintaining their fundamental structure due to the
567 exceptional stability of rare earth phosphates under reducing conditions. TiO_2 NPs revealed very

similar resistance to weathering and a relatively simple composition dominated by Ti and O with minor Ca association (Fig. A10), suggesting manufactured TiO_2 nanomaterials rather than naturally occurring titanium minerals (Kiser et al. 2009). The compositional purity and lack of elements typically associated with natural titanium minerals (Fe, Al, Si) provide compelling evidence for an anthropogenic origin (Karkee and Gundlach-Graham, 2024), likely from consumer products such as cosmetics, sunscreens, paints, and food additives. This conclusion aligns with research by Kiser et al. (2009) and Westerhoff et al. (2011), who traced similar TiO_2 signatures in wastewater systems to consumer products. The SEM-EDS analysis of CuO NPs indicated compositional profiles that suggest multiple sources. The CAK sample contained numerous particles with a specific composition dominated by copper-chromium oxides (Fig. A11). This distinctive elemental signature strongly suggests industrial origins, most likely from metal finishing, electroplating, or pigment manufacturing processes (Feng et al. 2023). In contrast, naturally occurring Cu particles in sewage sludge exhibited a fundamentally different profile, with Cu present only as a minor component within the broader organo-mineral matrix (Fig. A12). Pb particles in the studied sludge samples can originate from various sources. While the corrosion of Pb pipes or components within the water distribution system is one potential contributor (Peng et al. 2022), the particles observed are probably characteristic of typical products resulting from anaerobic digestion and phosphate-stabilized waste systems (Fig. A13 and A14). The observed elemental associations, such as Pb with S and Cl (potentially forming PbS, $PbSO_4$ or chloropyromorphite, $Pb_5(PO_4)_3Cl$, respectively), align with the chemical transformations known to occur under the reducing conditions of anaerobic digestion and within phosphate-rich stabilization environments (Chen et al. 2021; Zeng et al. 2017). Analysis of Zn particles also revealed their predominant occurrence as zinc sulphide (ZnS), frequently incorporating or associating with various cations including Na, K, and Ca (Fig. A15). This composition represents the typical end-product of Zn transformation during anaerobic digestion, aligning with findings by Kim et al. (2014), who documented the prevalence of zinc sulphide forms in such environments. The transformation from diverse inputs—originating from sources like galvanized materials, personal care products, and tire wear—to ZnS is driven by the activity of sulphate-reducing bacteria and zinc's high affinity for sulphide, a process detailed by Lombi et al. (2012). However, some particles exhibit more complex compositions, incorporating elements like P, Al, and Fe, which suggests the presence of multiple Zn species or varied surface associations (Fig. A16). Interestingly, variations in Zn particle composition

were noted between different treatment plants; some showed simpler, sulphide-dominated forms, while others displayed these more complex elemental mixtures. These differences likely stem from variations in the initial Zn sources and overall wastewater characteristics specific to each catchment area.

3.4. Environmental risk assessment of metallic nanoparticles

To assess preliminary environmental risks of MNPs introduced to soil via sludge amendment, we compiled relevant toxicity data for the terrestrial environment (Table A17). Risk quotients (RQ), calculated as the ratio between predicted environmental concentrations (PEC) and predicted no-effect concentrations (PNEC), were used to evaluate potential ecological impacts. PEC values were derived using measured mass concentrations of NPs in sludge, assuming a standard application rate of 1.6 tons per hectare and soil characteristics (0.2 m mixing depth, 1500 kg m^{-3} density), yielding a soil mass of 3000 tons per hectare. PNEC values were derived from obtained toxicological benchmarks using the lowest values found in the literature for soil ecosystems. However, no toxicological data for PbO NPs were available; therefore, following the EU REACH methodology, values from bulk PbO were used with the highest assessment factor (1000) applied to account for the uncertainty (European Chemicals Agency, 2012).

Risk levels were classified as negligible ($RQ < 0.01$), low ($0.01 \leq RQ < 0.1$), moderate ($0.1 \leq RQ < 1$), or high ($RQ \geq 1$) based on calculated RQs. All MNPs exhibited negligible to low ecological risks across all samples (Fig. 5). Gold, Ce, and Ti showed consistently negligible risk profiles with RQ values below 0.01. While Cu and Ag demonstrated slightly higher values, they remained within the low-risk category, as did Pb and Zn. The latter two metals presented the highest RQ values among all analyzed metals, though still within the low-risk range, with maximum values observed in samples ZG and VG. These findings indicate that current application rates of sewage sludge pose minimal ecological risks from MNPs to soil ecosystems.

Figure 5.

Beyond the values used in the PEC/PNEC calculations, the ratios between the mass concentration of particulate NPs and the total mass concentration (particulate + dissolved) of indigenous metallic NPs in sludge samples obtained by sp-ICP-MS provide additional context for the interpretation of the

ecological risk assessments. The data reveal considerable differences in the ratios, indicating their specific tendency to partition between particulate and ionic forms. TiO_2 and CeO_2 NPs showed the highest ratios (2.48 and 0.68 respectively), suggesting greater stability and lower tendency to transform into dissolved species. PbO NPs (0.42), Au NPs (0.34) and CuO NPs (0.23) demonstrated intermediate ratios, while ZnO NPs and Ag NPs exhibited the lowest ratios (0.09 and 0.04, respectively). These findings align with previous spiking experiments that documented the dissolution behavior of Ag and ZnO NPs during the incubation stage. Although our assessment indicates that current sewage sludge application rates pose minimal ecological risks from MNPs, long-term projections or higher application rates warrant careful consideration (Wang et al. 2024). Continued applications could potentially elevate risk levels for resistant MNPs, while others like Ag and ZnO NPs may exert environmental impacts through the higher solubility and various leaching scenarios in the soil environment (Abbas et al. 2020; Kraas et al. 2017; Pradas del Real et al. 2016). Further investigation is essential, given the severe limitations in available nano-specific toxicity data (notably for PbO NPs) and the need for comprehensive long-term monitoring to validate these projections and ensure continued environmental safety.

4. Conclusions

This study presents a comprehensive analytical approach for the extraction, quantification and characterization of seven environmentally relevant MNPs (Ag, Au, CeO_2, CuO, PbO, TiO_2 and ZnO) in sewage sludge. Through a systematic evaluation of extraction methodologies, we identified 2.5 mM TSPP and a sludge-to-reagent ratio of 1:100 as the optimal extraction solution. This method provides consistently high performance in particle number recovery (>75%) and mass recovery (>84.5%) while maintaining particle size integrity for most NPs, as identified by sp-ICP-MS. This approach proved to be particularly valuable in investigating the occurrence and concentrations of MNPs in complex environmental matrices, as shown by the analysis of sludge samples from Croatian wastewater treatment plants.

Complementary SEM-EDS analysis revealed insights into nanoparticle composition and transformation pathways, detecting metal-specific associations with matrix components. Some metals underwent sulfidation processes—Ag, Pb and Zn formed AgS, PbS and ZnS, respectively—while others remained largely untransformed, such as Ce in REE-phosphate minerals and Ti in TiO_2.

The most MNPs currently present negligible to low ecological risks under present agricultural application scenarios. The differential tendencies of metallic NPs to remain in particulate form (TiO_2>CeO_2>PbO>Au>CuO>ZnO>Ag) provided additional context for interpreting ecological risks, suggesting that Ag and ZnO NPs may pose environmental risks primarily through their dissolution tendency in high-organic-rich environments. This integrated approach, combining multiple analytical techniques and evaluating complementary particle metrics, represents a significant advancement in environmental monitoring capabilities for MNPs as emerging contaminants.

CRediT authorship contribution statement

Mavro Lučić: Writing – original draft, Validation, Methodology, Investigation, Funding acquisition, Data curation, Conceptualization. **Radmila Milačič Ščančar**: Writing – review & editing, **Janez Ščančar**: Writing – review & editing, Funding acquisition. **Željka Fiket:** Writing – review & editing. **Bor Arah**: Data curation, Formal analysis. **Janja Vidmar**: Writing – review & editing, Conceptualization.

Declaration of Competing Interest

The authors declare that they have no known competing financial interests or personal relationships that could have appeared to influence the work reported in this paper.

Acknowledgements

This research was supported by the Slovenian Research and Innovation Agency – ARIS Program P1-0143. Mavro Lučić's research fellowship at the Jožef Stefan Institute was funded by the European Union – NextGenerationEU program. We gratefully acknowledge the staff of the wastewater treatment plants for their assistance in providing sludge samples. We extend special thanks to Dr. Marin Ganjto from the Zagreb WWTP for providing substantial sample quantities that enabled our method development, and to Dr. Hana Fajković for supplying sludge samples from the Velika Gorica WWTP.

Data Availability

The sp-ICP-MS data of the indigenous MNPs in the sewage sludge samples will be made publicly available on Zenodo at [DOI], licensed under the Creative Commons Attribution 4.0 International (CC BY 4.0) license.

References

682 Abbas, Q., Yousaf, B., Amina, Ali, M.U., Munir, M.A.M., El-Naggar, A., Rinklebe, J., Naushad, M.,
683 2020. Transformation pathways and fate of engineered nanoparticles (ENPs) in distinct interactive
684 environmental compartments: a review. Environ. Int. 138, 105646.
685 https://doi.org/10.1016/j.envint.2020.105646

686 Abbas, Q., Zia-ur-Rehman, M., Ullah, H., Munir, M.A.M., Ali, M.U., Ali, M., Pikon, K.,Yousaf, B., 2024.
687 Recent advances in the detection and quantification of manufactured nanoparticles (MNPs) in
688 complex environmental and biological matrices. J. Clean. Prod. 471, 143454.
689 https://doi.org/10.1016/j.jclepro.2024.143454

690 Baur, S., Reemtsma, T., Stärk, H.J., Wagner, S., 2020, Surfactant assisted extraction of incidental
691 nanoparticles from road runoff sediment and their characterization by single particle-ICP-MS.
692 Chemosphere. 246, 125765. https://doi.org/10.1016/j.chemosphere.2019.125765

693 Besha, A.T., Liu, Y., Bekele, D.N., Dong, Z., Naidu, R., Gebremariam, G.N., 2020. Sustainability and
694 environmental ethics for the applica tion of engineered nanoparticles. Environ. Sci. Policy. 103, 85–
695 98. https://doi.org/10.1016/j.envsci.2019.10.013

696 Bland, G.D., Lowry, G.V., 2020. Multistep Method to Extract Moderately Soluble Copper Oxide
697 Nanoparticles from Soil for Quantification and Characterization. Anal. Chem. 92, 9620−9628.
698 https://doi.org/10.1021/acs.analchem.0c00824

699 Borowska, M., Jankowski, K., 2023, Basic and advanced spectrometric methods for complete
700 nanoparticles characterization in bio/eco systems: current status and future prospects. Anal. Bioanal.
701 Chem. 415, 4023–4038. https://doi.org/10.1007/s00216-023-04641-7

702 Bundschuh, M., Filser, J., Lüderwald, S., McKee, M.S., Metreveli, G., Schaumann, G.E., Schulz, R.,
703 Wagner, S., 2018. Nanoparticles in the environment: where do we come from, where do we go to?
704 Environ. Sci. Eur. 30, 1–17. https://doi.org/10.1186/s12302-018-0132-6

705 Cervantes-Avilés, P., Huang, X., Keller, A.A., 2021. Dissolution and Aggregation of Metal Oxide
706 Nanoparticles in Root Exudates and Soil Leachate: Implications for Nanoagrochemical Application.
707 Environ. Sci. Technol. 55, 20, 13443–13451. https://doi.org/10.1021/acs.est.1c00767

Chen, Z., Xing, R., Yang, Y., Zhao, Z., Liao, H., Zhou, S., 2021. Enhanced in situ Pb (II) passivation by biotransformation into chloropyromorphite during sludge composting. J. Hazard. Mater. 408, 124973. https://doi.org/10.1016/j.jhazmat.2020.124973

Council of the European Union. COUNCIL DIRECTIVE of 12 June 1986 on the protection of the environment, and in particular of the soil, when sewage sludge is used in agriculture, Offical Journal of the European Communities § (1986)

Dar, S.A., Balaram, V., Roy, P., Mir, A.R., Javed, M., Teja, M.S., 2025. Phosphorite deposits: A promising unconventional resource for rare earth elements (REEs). Geosci. Front. 102044. https://doi.org/10.1016/j.gsf.2025.102044

Diegoli, S., Manciulea, A.L., Begum, S., Jones, I.P., Lead, J.R., Preece, J.A., 2008. Interaction between manufactured gold nanoparticles and naturally occurring organic macromolecules. Sci. Total. Environ. 402, 1, 51–61. https://doi.org/10.1016/j.scitotenv.2008.04.023

El-Kalliny, A.S., Abdel-Wahed, M.S., El-Zahhar, A.A., Hamza, I.A., Gad-Allah, T.A., 2023. Nanomaterials: a review of emerging contaminants with potential health or environmental impact. Discov. Nano. 18, 68. https://doi.org/10.1186/s11671-023-03787-8

European Chemicals Agency, 2012. Guidance on Information Requirements and Chemical Safety Assessment. https://echa.europa.eu/guidance-documents/guidance-on-information-requirements-andchemical-safety-assessment (accessed 2025−05−13).

Eurostat, 2022. Sewage sludge production and disposal *[env_ww_spd]*. [Online].

Keller, A.A., Zheng, Y., Praetorius, A., Quik, J.T.K., Nowack, B., 2024. Predicting environmental concentrations of nanomaterials for exposure assessment - a review. NanoImpact. 33, 100496. https://doi.org/10.1016/j.impact.2024.100496

Feng, J., Burke, I.T., Chen, X., Stewart, D.I., 2023. Assessing metal contamination and speciation in sewage sludge: implications for soil application and environmental risk. Rev. Environ. Sci. Biotechnol. 22, 1037–1058. https://doi.org/10.1007/s11157-023-09675-y

Filipović, F., Grčić, I., Bermanec, V., Kniewald, G., 2013. Monitoring of total metal concentration in sludge samples: Case study for the mechanical–biological wastewater treatment plant in Velika Gorica, Croatia. Sci. Total. Environ. 447, 17-24. https://doi.org/10.1016/j.scitotenv.2012.12.078

Goodman, A.J., Benner, B.F., Montaño, M.D., 2025. Out of the lab and into the environment: the evolution of single particle ICP-MS over the past decade. Environ Sci: Nano. 3, 12, 1789-1800. https://doi.org/10.1039/D4EN00804A

Gomez-Gonzalez, M.A., Rehkämper, M., Han, Z., Ryan, M.P., Laycock, A., Porter, A.E., 2022. ZnO Nanomaterials and Ionic Zn Partition within Wastewater Sludge Investigated by Isotopic Labeling. Glob. Chall. 6, 2100091. https://doi.org/10.1002/gch2.202100091

Gray, E.P., Coleman, J.G., Bednar, A.J., Kennedy, A.J., Ranville J.F., Higgins, C.P., 2013, Extraction and analysis of silver and gold nanoparticles from biological tissues using single particle inductively coupled plasma mass spectrometry. Environ. Sci. Technol. 47, 14315–14323. https://doi.org/10.1021/es403558c

Jiang, J., Wang, X., Zhang, Y., Zhang, J., Gu, X., He, S., Duan, S., Ma, J., Wang, L., Luo, P., 2022. The Aggregation and Dissolution of Citrate−Coated AgNPs in High Ammonia Nitrogen Wastewater and Sludge from UASB−Anammox Reactor. Int. J. Environ. Res. Public Health. 19, 15, 9502. https://doi.org/10.3390/ijerph19159502

Karkee, H., Gundlach-Graham, A., 2024, Two-stage hierarchical clustering for analysis and classification of mineral sunscreen and naturally occurring nanoparticles in river water using single-particle ICP-TOFMS. Environ. Sci.: Nano. 11, 4162−4173. https://doi.org/10.1039/D4EN00288A

Keller, A.A., Adeleye, A.S., Conway, J.R., Garner, K.L., Zhao, L., Cherr, G.N., Hong, J., Gardea-Torresdey, J.L., Godwin, H.A. and Hanna, S. et al., 2017. Comparative environmental fate and toxicity of copper nanomaterials. NanoImpact. 7, 28–40. https://doi.org/10.1016/j.impact.2017.05.003

Kim, B., Levard, C., Murayama, M., Brown, G.E., Jr. Hochella, M.F.Jr., 2014. Integrated Approaches of X-Ray Absorption Spectroscopic and Electron Microscopic Techniques on Zinc Speciation and Characterization in a Final Sewage Sludge Product. J. Environ. Qual. 43, 908-916. https://doi.org/10.2134/jeq2013.10.0418

760 Kiser, M.A., Westerhoff, P., Benn, T., Wang, Y., Perez-Rivera, J., Hristovski, K., 2009, Titanium
761 nanomaterial removal and release from wastewater treatment plants. Environ. Sci. Technol. 43, 17,
762 6757–6763. https://doi.org/10.1021/es901102n

763 Kraas, M., Schlich, K., Knopf, B., Wege, F., Kägi, R., Terytze, K. and Hund-Rinke, K., 2017, Long-
764 term effects of sulfidized silver nanoparticles in sewage sludge on soil microflora. Environ. Toxicol.
765 Chem. 36, 3305-3313. https://doi.org/10.1002/etc.3904

766 Laborda, F., Bolea, E., Jiménez-Lamana, J., 2014, Single Particle Inductively Coupled Plasma Mass
767 Spectrometry: A Powerful Tool for Nanoanalysis. Anal. Chem. 86, 5, 2270–2278.
768 https://doi.org/10.1021/ac402980q

769 Laycock, A., Clark, N.J., Clough, R., Smith, R., Handy, R.D., 2022, Determination of metallic
770 nanoparticles in biological samples by single particle ICP-MS: A systematic review from sample
771 collection to analysis. Environ. Sci.: Nano. 2, 9. 420–453. https://doi.org/10.1039/D1EN00680K

772 Li, D., Zhou, Y., Tan, Y., Pathak, S., bin Abdul Majid, M., Ng, W.J., 2016. Alkali-solubilized organic
773 matter from sludge and its degradability in the anaerobic process. Bioresour. Technol. 200, 579–586.
774 https://doi.org/10.1016/j.biortech.2015.10.083

775 Lockwood, T.E., Gonzalez De Vega, R., Clases, D., 2021. An interactive Python-based data
776 processing platform for single particle and single cell ICP-MS. J. Anal. At. Spectrom. 36, 2536–2544.
777 https://doi.org/10.1039/D1JA00297J

778 Lombi, E., Donner, E., Tavakkoli, E., Turney, T.W., Naidu, R., Miller, B.W., Scheckel, K.G., 2012. Fate
779 of Zinc Oxide Nanoparticles during Anaerobic Digestion of Wastewater and Post-Treatment
780 Processing of Sewage Sludge. Environ. Sci. Technol. 46, 16, 9089-9096.
781 https://doi.org/10.1021/es301487s

782 Moreno-Martín, G., Gómez-Gómez, B., León-González, M.E., Madrid, Y., 2022. Characterization of
783 AgNPs and AuNPs in sewage sludge by single particle inductively coupled plasma-mass
784 spectrometry. Talanta. 238, 123033. https://doi.org/10.1016/j.talanta.2021.123033

785 Mudunkotuwa, I.A., Rupasinghe, T., Wu, C.-M., Grassian, V.H., 2011. Dissolution of ZnO
786 Nanoparticles at Circumneutral pH: A Study of Size Effects in the Presence and Absence of Citric
787 Acid. Langmuir. 28, 1, 396–403. https://doi.org/10.1021/la203542x

788 Ng, D.Q., Chu, Y., Tan, S.W., Wang, S.L., Lin, Y.P., Chu, C.H. Soo, Y-L., Song, Y-F., Chen, P-J.,
789 2018. In vivo evidence of intestinal lead dissolution from lead dioxide (PbO_2) nanoparticles and
790 resulting bioaccumulation and toxicity in medaka fish. Environ. Sci.: Nano. 6, 2, 580–591.
791 https://doi.org/10.1039/C8EN00893K

792 Nowack, B., 2017. Evaluation of environmental exposure models for engineered nanomaterials in a
793 regulatory context. NanoImpact. 8, 38-47. https://doi.org/10.1016/j.impact.2017.06.005

794 Pace, H.E., Rogers, N.J., Jarolimek, C., Coleman, V.A., Higgins, C.P., Ranville J.F., 2011.
795 Determining transport efficiency for the purpose of counting and sizing nanoparticles via single
796 particle inductively coupled plasma mass spectrometry. Anal. Chem. 83, 9361–9369.
797 https://doi.org/10.1021/ac201952t

798 Peng, Y.-C., Lu, Y.-F., Lin, Y.-P., 2022. Release of Particulate Lead from Four Lead Corrosion
799 Products in Drinking Water: A Laboratory Study Coupled with Microscopic Observations and
800 Computational Fluid Dynamics. Environ. Sci. Techol. 56, 17, 12218-12227.
801 https://doi.org/10.1021/acs.est.2c02461

802 Pradas del Real, A.E., Castillo-Michel, H., Kaegi, R., Sinnet, B., Magnin, V., Findling, N., Villanova, J.,
803 Carrière, M., Santaella, C., Fernández-Martínez, A., Levard, C., Sarret, G., 2016. Fate of Ag-NPs in
804 Sewage Sludge after Application on Agricultural Soils. Environ. Sci. Technol. 50, 4, 1759–1768.
805 https://doi.org/10.1021/acs.est.5b04550

806 Pranudta, A., Chanthapon, N., Kidkhunthodc. P., El-Moselhy, M.M., Nguyen, T.T., Padungthon, S.,
807 2021. Selective removal of Pb from lead-acid battery wastewater using hybrid gel cation exchanger
808 loaded with hydrated iron oxide nanoparticles: Fabrication, characterization, and pilot-scale validation.
809 J. Environ. Chem. Eng. 9, 5, 106282. https://doi.org/10.1016/j.jece.2021.106282

810 R core team, 2023. R: a language and environment for statistical computing. R Foundation for
811 statistical computing, Vienna, Austria. http://www.R-project.org

812 Rippner, D.A., Margenot, A.J., Fakra, S.C., Aguilera, L.A., Sohng, J., Dynarski K.A., Waterhouse, H.,
813 McElroy, N., Wade, J., Hind, S.R., Green, P.G., Peak, D., McElrone, A.J., Chen, N., Feng, R., Scow,
814 K.M., Parikh, S.J., 2021.Microbial response to copper oxide nanoparticles in soils is controlled by land
815 use rather than copper fate. Environ. Sci.: Nano. 8, 3560-3576. https://doi.org/10.1039/D1EN00656H

816 Salehi, M., Beni, O.H., Harchegani, H.B., Borujeni, I.E., Motaghian, H., 2011. Refining soil organic
817 matter determination by loss-on-ignition. Pedosphere. 21, 473–482. https://doi.org/10.1016/S1002-
818 0160(11)60149-5

819 Schwertfeger, D.M., Velicogna, J.R., Jesmer, A.H., Saatcioglu, S., McShane, H., Scroggins, R.P.,
820 Princz, J.I., 2017. Extracting metallic nanoparticles from soils forquantitative analysis: method
821 development using engineered silver nanoparticlesand SP-ICP-MS. Anal. Chem. 89, 4, 2505–2513.
822 https://doi.org/10.1021/acs.analchem.6b04668

823 Tou, F., Niu, Z., Fu, J., Wu, J., Liu, M., Yang, Y., 2021. Simple Method for the Extraction and
824 Determination of Ti-, Zn-, Ag-, and Au-Containing Nanoparticles in Sediments Using Single-Particle
825 Inductively Coupled Plasma Mass Spectrometry. Environ. Sci. Technol. 55, 15, 10354–10364.
826 https://doi.org/10.1021/acs.est.1c00983

827 Tou, F., Yang, Y., Feng, J., Niu, Z., Pan, H., Qin, Y., Guo, X., Meng, X., Liu, M., Hochella, M. F., 2017.
828 Environmental Risk Implications of Metals in Sludges from Waste Water Treatment Plants: The
829 Discovery of Vast Stores of Metal Containing Nanoparticles. Environ. Sci. Technol. 51, 9, 4831−4840.
830 https://doi.org/10.1021/acs.est.1c00983

831 U. S. Environmental Protection Agency. Basic Information about Biosolids. https://www. epa.gov/
832 biosolids/basic-information-about-biosolids#uses accessed 12 March 2025.

833 Vidmar, V., Milačič Ščančar, R., Ščančar, J., 2017. Sizing and simultaneous quantification of
834 nanoscale titanium dioxide and a dissolved titanium form by single particle inductively coupled plasma
835 mass spectrometry. Microchem. J. 132, 391–400. https://doi.org/10.1016/j.microc.2017.02.030

836 Vidmar, J., Zuliani, T., Milačič, R., Ščančar, J., 2022. Following the Occurrence and Origin of Titanium
837 Dioxide Nanoparticles in the Sava River by Single Particle ICP-MS. Water. 14, 6, 959.
838 https://doi.org/10.3390/w14060959

Wang, J., Zhao, X., Wu, F., Tang, Z., Zhao, T., Niu, L., Fang, M., Wang, H., Wang, F., 2021. Impact of montmorillonite clay on the homo- and heteroaggregation of titanium dioxide nanoparticles ($nTiO_2$) in synthetic and natural waters. Sci. Total. Environ. 784, 147019. https://doi.org/10.1016/j.scitotenv.2021.147019

Westerhoff, P., Lee, S., Yang, Y., Gordon, G.W., Hristovski, K., Halden, R.U., Herckes, P., 2015. Characterization, Recovery Opportunities, and Valuation of Metals in Municipal Sludges from U.S. Wastewater Treatment Plants Nationwide. Environ. Sci. Technol. 49, 16, 9479–88. https://doi.org/10.1021/es505329g

Westerhoff, P.K., Song, G., Hristovski, K., and Kiser, A., 2011. Occurrence and removal of titanium at full scale wastewater treatment plants: Implications for TiO2 nanomaterials. J. Environ. Monit. 13, 1195–1203. https://doi.org/10.1039/C1EM10017C

Wu, F., Harper, B.J., Harper, S.J., 2019. Comparative dissolution, uptake, and toxicity of zinc oxide particles in individual aquatic species and mixed populations. Environ. Toxicol. Chem. 38, 3, 591–602. https://doi.org/10.1002/etc.4349

Yang, Y., Chen, B., Hower, J., Schindler, M., Winkler, C., Brandt, J., Di Giulio, R., Ge, J., Liu, M., Fu, Y., Zhang, L., Chen, Y., Priya, S., Hochella, M.F. Jr., 2017. Discovery and ramifications of incidental Magnéli phase generation and release from industrial coal-burning. Nat. Commun. 8, 194. https://doi.org/10.1038/s41467-017-00276-2

Zeng, G., Wan, J., Huang, D., Hu, L., Huang, C., Cheng, M., Xue, W., Gong, X., Wang, R., Jiang, D., 2017. Precipitation, adsorption and rhizosphere effect: the mechanisms for phosphate-induced Pb immobilization in soils—a review. J. Hazard. Mater. 339, 354–367. https://doi.org/10.1016/j.jhazmat.2017.05.038

Figure 1. Bar graphs show the percentage recovery of six MNPs (Au, Ag, CeO_2, CuO, PbO and TiO_2) in different extraction solutions: Mili-Q water; 2.5; 10; and 20 mM TSPP. The error bars represent the standard deviation of at least two measurements.

Figure 2. Bar graphs show the percentage recovery of six metallic NPs (Au, Ag, CeO_2, CuO, PbO and TiO_2) using 2.5 mM TSPP as the optimal extraction solution. The error bars represent the standard deviation of five measurements.

Figure 3. Particle number concentrations of Ag-, Au-, CeO_2-, CuO-, PbO-, TiO_2-, and ZnO-based NPs in sewage sludge samples in Croatia.

Figure 4. The size distribution of Ag-, Au-, CeO_2-, CuO-, PbO-, TiO_2-, and ZnO-based NPs in the samples containing their highest particle concentrations. The highest concentrations were found for Au, Ag, TiO_2, and ZnO in VG sample; CeO_2 in SIS sample; and CuO and PbO in ZG sample.

Figure 5. Results of risk quotient (RQ) calculation. Results can be interpreted as follow: (I) $RQ < 0.01$: Negligible risk; (II) $0.01 \leq RQ < 0.1$: Low risk; (III) $0.1 \leq RQ < 1$: Moderate risk; (IV) $RQ \geq 1$: High risk.

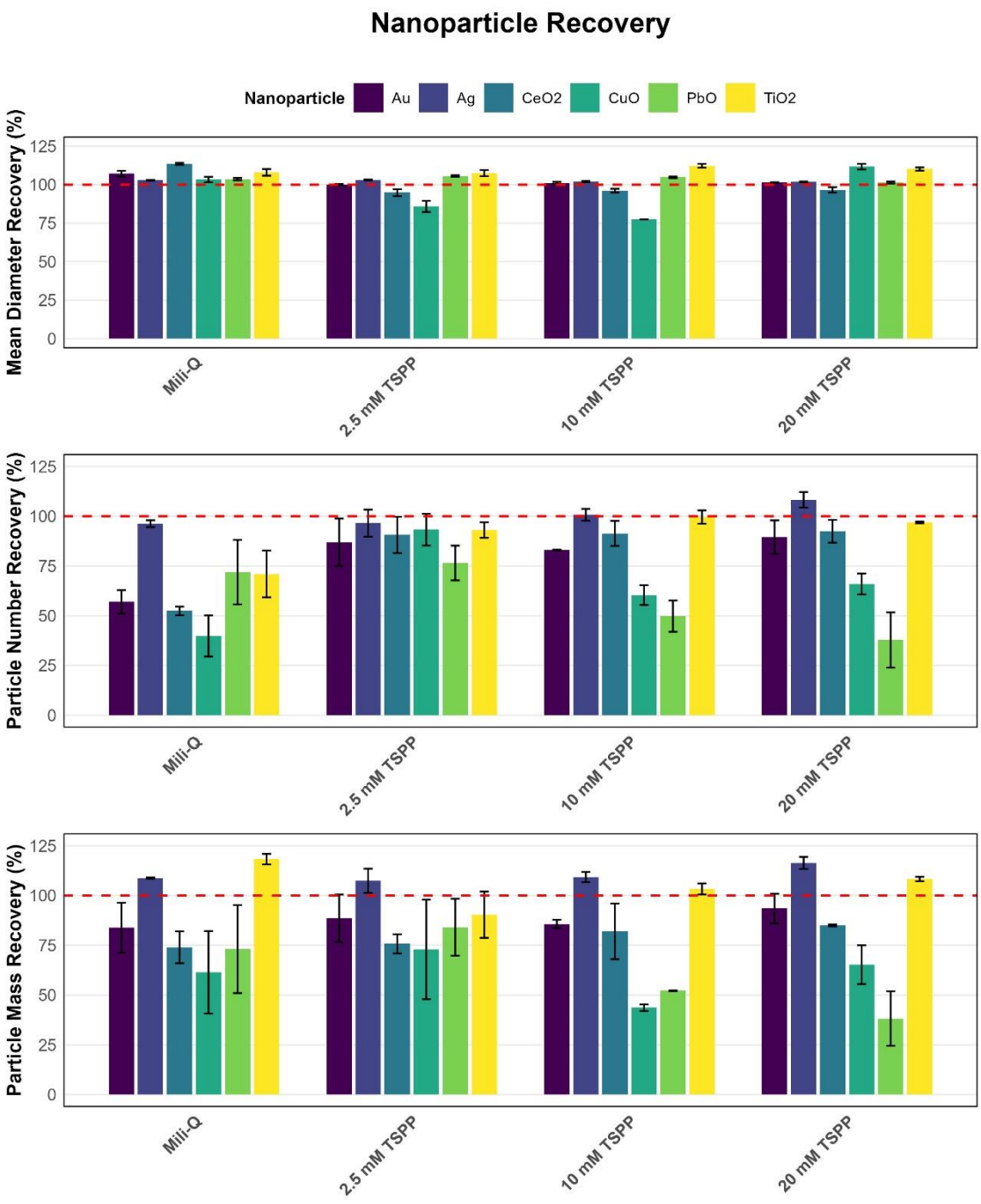
Nanoparticle Recovery
Nanoparticle
Au
Ag
CeO2
CuO
PbO
TiO2
Mean Diameter Recovery (%)
Particle Number Recovery (%)
Particle Mass Recovery (%)
0
25
50
75
100
125
Mili-Q
2.5 mM TSPP
10 mM TSPP
20 mM TSPP

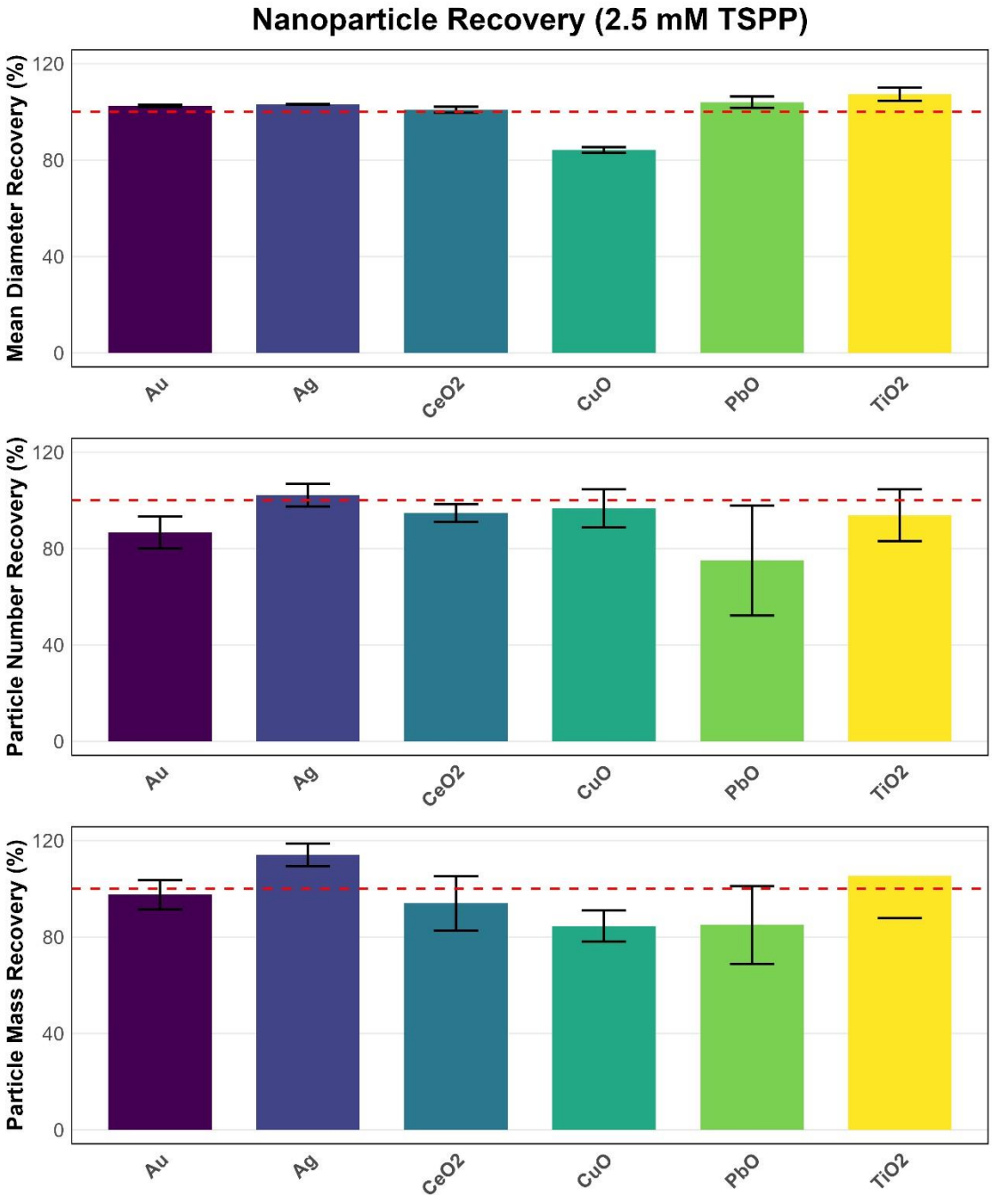
Nanoparticle Recovery (2.5 mM TSPP)
Mean Diameter Recovery (%)
Particle Number Recovery (%)
Particle Mass Recovery (%)
120
80
40
0
Au
Ag
CeO2
CuO
PbO
TiO2

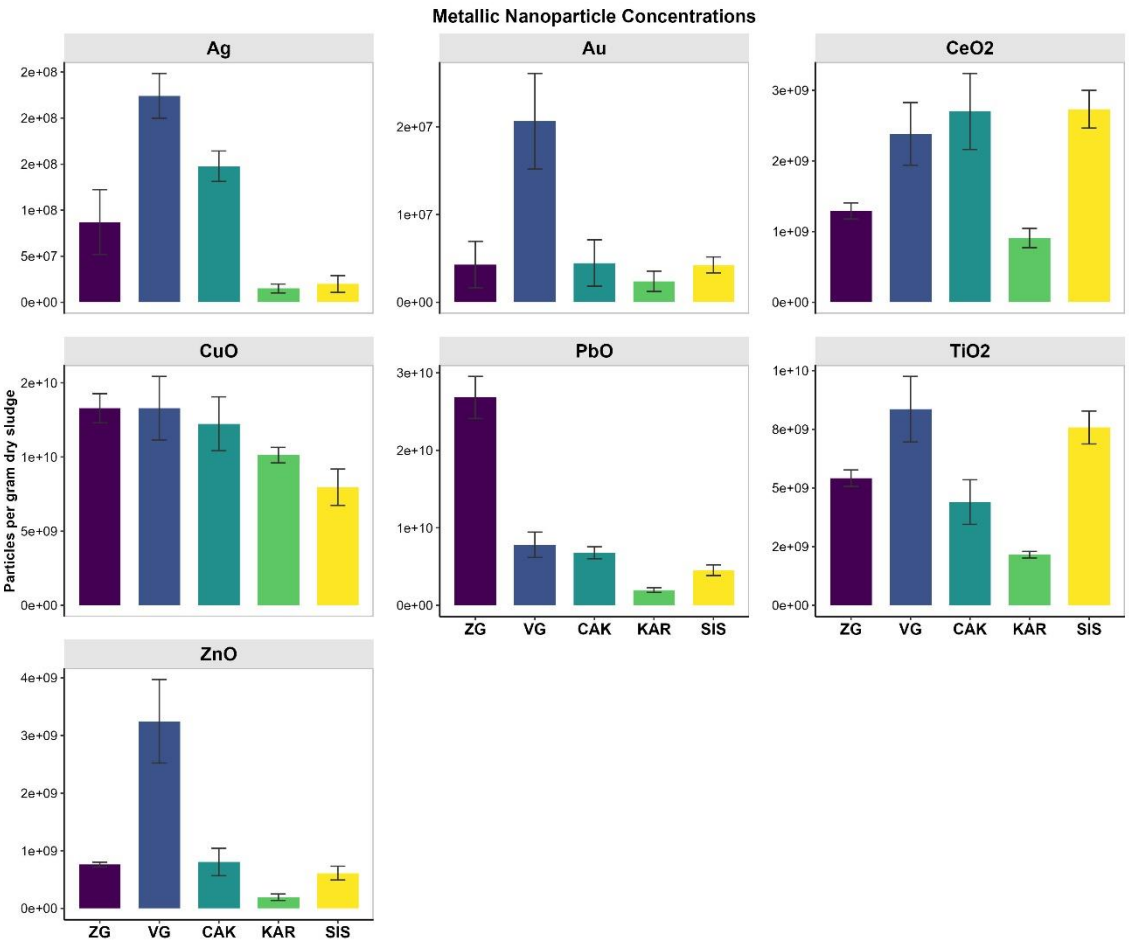
Metallic Nanoparticle Concentrations
Ag
Au
CeO2
CuO
PbO
TiO2
ZnO
Particles per gram dry sludge
ZG
VG
CAK
KAR
SIS

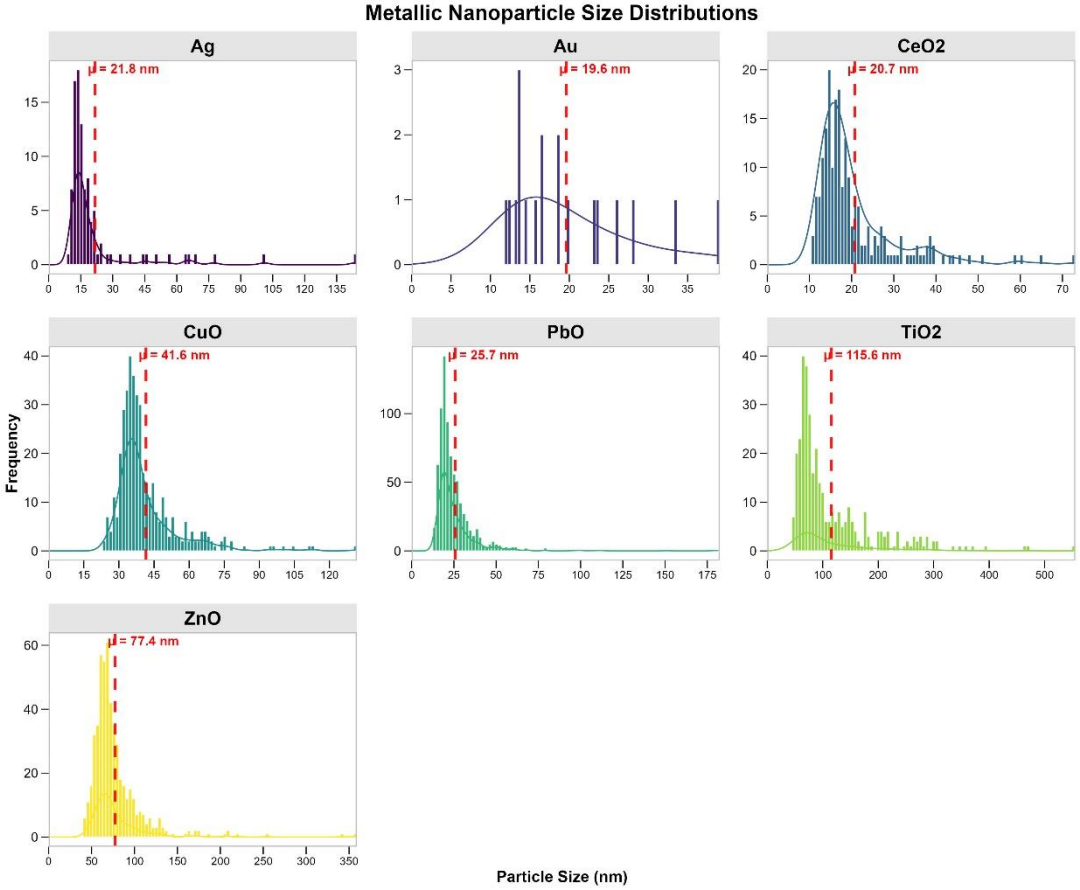
Metallic Nanoparticle Size Distributions
Ag
μ = 21.8 nm
Au
μ = 19.6 nm
CeO2
μ = 20.7 nm
CuO
μ = 41.6 nm
PbO
μ = 25.7 nm
TiO2
μ = 115.6 nm
ZnO
μ = 77.4 nm
Frequency
Particle Size (nm)

4

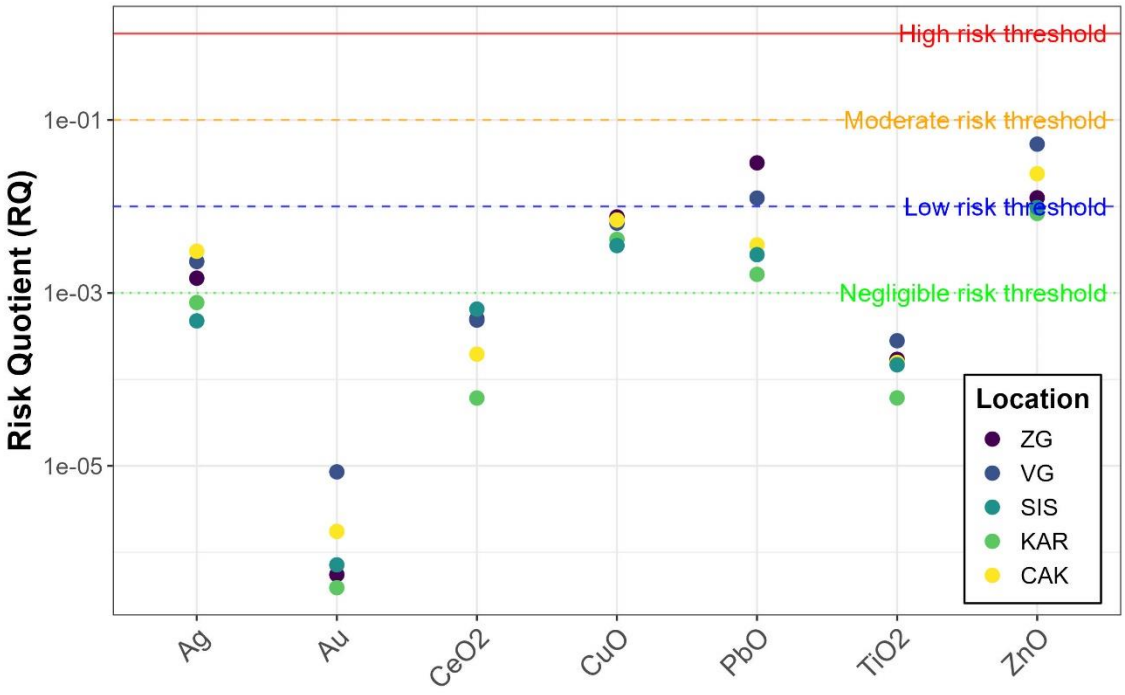
High risk threshold
Moderate risk threshold
Low risk threshold
Negligible risk threshold
Risk Quotient (RQ)
1e-01
1e-03
1e-05
Ag
Au
CeO2
CuO
PbO
TiO2
ZnO
Location
ZG
VG
SIS
KAR
CAK